A ROBUST SIGNAL-FLOW ARCHITECTURE
FOR COOPERATIVE VEHICLE DENSITY CONTROL

Thomas A. Baran★   *Berthold K. P. Horn*†

Massachusetts Institute of Technology
★Digital Signal Processing Group, Research Laboratory of Electronics
†Computer Science and Artificial Intelligence Laboratory

ABSTRACT

Traffic flow instabilities have many potential negative consequences, including increased danger of collisions, higher fuel consumption, faster of abrasion of roadways, and reduction of overall traffic throughput. Instabilities occur even if modern forward-looking adaptive cruise control systems are used. In this paper, we present an architecture for controlling vehicle density that uses coordination between adjacent vehicles to attain desired safe following distances, without generating these types of instabilities in the process. The presented architecture has several additional desirable properties, including being robust to sensor failures and measurement inconsistencies, as well as allowing for inhomogeneous vehicle dynamics.

Index Terms— Traffic flow instabilities, cooperative control, conservation.

1. INTRODUCTION

We are all only too familiar with traffic flow instabilities, including alternating stop-and-go driving conditions. A variety of simple models of traffic flow predict waves of density and speed moving along roadways, e.g. [1–30], particularly at higher traffic density. As is discussed in [31], a primary root cause is drivers' feedback control of vehicles. Even with modern forward-looking adaptive cruise control systems, the cascade of many such systems will tend to increasingly amplify perturbations as they are passed down a chain of vehicles, resulting in an overall instability.

This paper presents a signal-flow architecture for controlling the distances between vehicles in a chain, and doing so in a way that avoids the type of instabilities previously mentioned. The architecture also has several other attractive properties, including the ability to incorporate an absolute maximum speed limit, the ability to allow for inhomogeneous safe following distances, and the ability to allow for diverse vehicle dynamics. Potential system failures, e.g. sensor inaccuracies and sensor failures, can often be handled without having catastrophic results. It is in this sense that the presented architecture is considered to be robust. [32] The architecture, which is based upon localized measurements and communication between adjacent vehicles, may be viewed as a cooperative control algorithm. [33] A centralized control mechanism is not required.

2. GENERAL ARCHITECTURE

The general signal-flow architecture is depicted in Fig. 2(a), with the variable N being used to denote the number of vehicles in the chain. It is formulated as a continuous-time system, with the time index omitted from signals in this figure for clarity. We will use a moving reference frame, so that a chain of vehicles traveling at a target velocity with respect to the road is moving at zero velocity with respect to the reference frame.

Each gray region in Fig. 2(a) represents a vehicle in the chain and encompasses the sensors, speed control dynamics, and signal processing used in implementing the portion of the architecture that resides in that vehicle. In an intermediate vehicle in the chain, a particular vehicle k operates by measuring its respective front-facing and rear-facing inter-vehicle distances $d_k(t)$ and $d_{k+1}(t)$, applying respective memoryless nonlinearities f_k and g_k to the measurements, and performing the additions, subtractions and distributions indicated in the figure. This includes transmitting signals to adjacent vehicles and receiving signals from adjacent vehicles, e.g. via a wireless link. In each vehicle, a command signal $b_{3k-2}(t)$ is sent to the system h_k, which incorporates the vehicle speed control mechanism in addition to the vehicle dynamics. Each function h_k may generally be non-linear, time-varying and may contain memory, with the key requirement being that it satisfies the following condition, expressed as a relationship between the signal $b_{3k-2}(t)$ and the vehicle velocity denoted $v_k(t) = da_{3k-2}(t)/dt$:

$$\mathrm{sign}\left(b_{3k-2}(t)\right) = \mathrm{sign}\left(v_k(t)\right). \tag{1}$$

In this sense, the attractive properties of the presented signal-flow architecture pertain to a vehicle chain where the dynamics of each individual vehicle may belong to a broad class.

An example of a function h_k that satisfies Eq. 1 is a continuous-time integrator, realized as a cruise control mechanism that instantaneously sets the vehicle velocity, measured within the moving reference frame, to the value of $b_{3k-2}(t)$. The system may also incorporate a mechanism to limit the maximum allowable velocity. Described in this way, the example system requires the ability to instantaneously change velocity and therefore is impossible to realize in a physical vehicle in practice. However we emphasize that the condition in Eq. 1, which is a condition on signals, can be satisfied, e.g. if the input signals b_{3k-2} are sufficiently smooth and vary sufficiently slowly with respect to the response time of the system h_k.

Fig. 2(b-c) illustrates some example alternative realizations of systems within the presented architecture, obtained by setting certain of the memoryless nonlinearities f_k and g_k to zero. As will be discussed in Subsection 3.2, all systems within the architecture, including those in Fig. 2(b-c), will exhibit desirable stability properties. The systems in Fig. 2(b-c) therefore serve to illustrate one sense in which the architecture is robust. In particular, if loss of a sensor is detected, the associated memoryless nonlinearity can be set to zero, resulting not in a catastrophic situation but rather in another realization of a system within the presented architecture.

3. CONSERVATION AND VARIATIONAL PRINCIPLES

The key arguments underlying the stability, robustness and transient behavior of the presented architecture are formulated using the general approach discussed in [34]. Broadly speaking, the arguments in [34] are based on the idea that when a signal processing algorithm exhibits a conservation principle resembling the form of power conservation in physical systems, e.g. in electrical networks, the algorithm will also typically exhibit many of the desirable properties of those systems, e.g. the many results in [35]. A critical point with the line of reasoning in [34] is that a reference physical system is not required in relating the structure of the algorithm to conservation and the associated desirable properties. The identification and synthesis of conservation principles are instead often a matter of appropriately organizing algorithm variables so that the equations describing conservation naturally emerge, independent of whether the equations describe a particular physical system of interest.

The key property that we derive from this perspective is that a system constructed according to the presented architecture will tend toward a minimum point of an overall potential function related to inter-vehicle distance. This behavior is reminiscent of the principle of minimum heat, and more generally the so-called principles of decreasing content and co-content, in electrical networks. [36–38] As the property relates changes in individual vehicles to variations in an overall potential function, it provides a method for analyzing the way that a specific vehicle affects other vehicles in the system. In particular, the variational perspective facilitates the analysis of the dynamics of the overall system in recovering from perturbations resulting from, e.g., changes in the desired inter-vehicle distances, changes in the desired speeds, unexpected braking, or temporary system malfunctions.

3.1. Conservation principle

Following the general approach in [34], we proceed by identifying an organization of the variables in the system in Fig. 2(a) that results in a pair of orthogonal vector spaces. Referring to this figure, the claims in particular are that:

(C1) The vector of variables $a_k(t)$ lies, for all time, in a vector subspace of $\mathbb{R}^{3N-2}$ denoted A,

(C2) The vector of variables $b_k(t)$ lies, for all time, in a vector subspace of $\mathbb{R}^{3N-2}$ denoted B, and

(C3) The vector subspaces A and B are orthogonal.

Denoting the vector of variables $a_k(t)$ as

$$\underline{a}(t) = [a_1(t), \ldots, a_{3N-2}(t)]^T \tag{2}$$

and the vector of variables $b_k(t)$ as

$$\underline{b}(t) = [b_1(t), \ldots, b_{3N-2}(t)]^T, \tag{3}$$

(C1)-(C3) can be written formally as

$$\underline{a}(t) \in A \subseteq \mathbb{R}^{3N-2}, \quad \forall t \tag{4}$$

$$\underline{b}(t) \in B \subseteq \mathbb{R}^{3N-2}, \quad \forall t \tag{5}$$

$$\langle \underline{a}, \underline{b} \rangle = 0, \quad \forall \underline{a} \in A, \underline{b} \in B. \tag{6}$$

In Eq. 6, $\langle \underline{a}, \underline{b} \rangle$ is used to denote the standard inner product on the corresponding real vector space of column vectors.

Demonstrating that Eqns. 4-6 hold is facilitated by rearranging the system in Fig. 2(a) so that it takes a form where the linear, memoryless interconnecting structure is represented using a signal-flow

graph, as depicted in Fig. 3. Following the convention in [39], signals corresponding to multiple incident branches directed toward a node are summed. Referring to Fig. 3, it is straightforward to verify the validity of Eq. 4 by noting that for all time, the variables $a_k(t)$ are related via the memoryless, linear signal-flow graph that is depicted in the top portion of that figure, and consequently a vector composed of these variables lies in a vector subspace $A \subseteq \mathbb{R}^{3N-2}$. Similarly, Eq. 5 is verified by observing that the variables $b_k(t)$ are related via the memoryless, linear signal-flow graph depicted in the bottom portion of Fig. 3, and consequently a vector composed of these variables lies in a vector subspace $B \subseteq \mathbb{R}^{3N-2}$.

The key observation used in verifying the validity of Eq. 6 is that the memoryless, linear signal-flow graph interconnecting the variables $b_k(t)$ in the bottom portion of Fig. 3 is the negative transpose of the memoryless, linear signal-flow graph interconnecting the variables $a_k(t)$ in the top portion of that figure. Still referring to this figure, we denote the vector of input variables to the top interconnection; the vector of output variables from the bottom interconnection; the vector of input variables to the bottom interconnection; and the vector of output variables from the bottom interconnection respectively as

$$\underline{c}_a = [a_1, a_4, a_7, \ldots, a_{3N-5}, a_{3N-2}]^T, \tag{7}$$

$$\underline{d}_a = [a_2, a_3, a_5, a_6, \ldots, a_{3N-4}, a_{3N-3}]^T, \tag{8}$$

$$\underline{c}_b = [b_2, b_3, b_5, b_6, \ldots, b_{3N-4}, b_{3N-3}]^T, \tag{9}$$

$$\underline{d}_b = [b_1, b_4, b_7, \ldots, b_{3N-5}, b_{3N-2}]^T. \tag{10}$$

Using Eqns. 7-10, the relationship between the inputs and outputs in the top interconnection in Fig. 3 can be written as

$$\underline{d}_a = \mathcal{G}\underline{c}_a, \tag{11}$$

with $\mathcal{G}$ denoting a matrix that encodes the memoryless, linear function implemented by the top interconnection graph. As the bottom interconnection in Fig. 3 is the negative transpose of the top interconnection in that figure, the relationship between the inputs and outputs in the bottom interconnection can be written as

$$\underline{d}_b = -\mathcal{G}^T \underline{c}_b. \tag{12}$$

Writing the expression for the inner product between the vectors $\underline{a}$ and $\underline{b}$, rearranging terms, substituting in the expressions in Eqns. 7-10, and substituting in the expressions in Eqns. 11 and 12 results in

$$\langle \underline{a}, \underline{b} \rangle = a_1 b_1 + \cdots + a_{3N-2} b_{3N-2} \tag{13}$$

$$= a_2 b_2 + a_3 b_3 + a_5 b_5 + a_6 b_6 + \cdots + a_{3N-3} b_{3N-3}$$
$$+ a_1 b_1 + a_4 b_4 + a_7 b_7 + \cdots + a_{3N-2} b_{3N-2} \tag{14}$$

$$= \underline{d}_a^T \underline{c}_b + \underline{c}_a^T \underline{d}_b \tag{15}$$

$$= \underline{c}_a^T \mathcal{G}^T \underline{c}_b - \underline{c}_a^T \mathcal{G}^T \underline{c}_b \tag{16}$$

$$= 0. \tag{17}$$

From the perspective of the behavior of the interconnection, the vector of inputs $\underline{c}_a$ is uncoupled from the vector of inputs $\underline{c}_b$, i.e. the constraints coupling the two vectors of input variables $\underline{c}_a$ and $\underline{c}_b$ in Fig. 3 are imposed not by the linear interconnecting systems, but rather by the functions f_k, g_k and h_k. From this, in addition to the fact that the vectors $\underline{a}$ and $\underline{b}$ individually lie in vector subspaces, it can be concluded that Eqns. 13-17 represent a statement of subspace orthogonality. The relationship between orthogonality of vector subspaces and the structure of signal-flow graphs is discussed in greater detail in Section 4.3 of [34].

Eq. 13 is also illustrative of the sense in which Eqns. 4-6 are regarded as a conservation principle. Specifically, the form of Eq. 13 resembles the expression for power conservation in physical systems, e.g. electrical networks. We emphasize, however, that Eqns. 4-6 represent conservation of a quantity that is non-physical, in the sense that the meaning and units of the $a_k b_k$ product is not necessarily that of power, nor any other physical quantity. I.e. the variables a_k may naturally represent units of length, although the variables b_k represent signals internal to each vehicle that can have somewhat arbitrary units or that may be unitless. The conservation principle emerges in the presented architecture not as a consequence of a fundamental physical law but rather as a consequence of the specific interconnection that was selected in its development.

3.2. Variational principle

As is discussed in [34], the existence of a physical or non-physical conservation principle that takes the form of Eqns. 4-6 often facilitates the identification of variational principles that can be used to characterize the behavior of the associated system. In the case of the system depicted in Fig. 3, Eqns. 1, 4, 5, and 6 imply that the system will tend toward a point of minimum local cost of the following constrained minimization problem:

$$\min_{x_1,\ldots,x_N} \quad G_1(d_2) + F_N(d_N) + \sum_{k=2}^{N-1} F_k(d_k) + G_k(d_{k+1}).$$

$$\text{s.t.} \quad d_2 = x_1 - x_2$$
$$\vdots \quad\quad\quad\quad\quad (18)$$
$$d_N = x_{N-1} - x_N$$
$$x_1 = 0$$

The functions $F_k(d_k)$ and $G_k(d_k)$ denote the integrals of the respective memoryless, nonlinear functions f_k and g_k. In particular,

$$F_k(y) \quad = \quad \int^y f_k(\tau)d\tau \quad\quad (19)$$

$$G_k(y) \quad = \quad \int^y g_k(\tau)d\tau, \quad\quad (20)$$

with the lower limits of integration in Eqns. 19-20 being an arbitrary value that is related to a constant term added to the functions F_k and G_k, consequently having no effect on the values of the variables x_k for which (18) is minimized.

We demonstrate that the cost in (18) is nonincreasing by first noting that the conservation principle in Eqns. 4-6 implies

$$\langle d\underline{a}(t)/dt, \underline{b}(t)\rangle = 0, \forall t. \quad\quad (21)$$

We will use $a'_k(t) = da_k(t)/dt$ and $b'_k(t) = db_k(t)/dt$ to denote the time derivatives of the respective signals $a_k(t)$ and $b_k(t)$. Referring to Fig. 3, the term $a'_1(t)b_1(t)$ evaluates to zero, and Eq. 21 can be written in the form of Eq. 14 as

$$0 = a'_2(t)b_2(t) + a'_3(t)b_3(t) + \cdots + a'_{3N-3}(t)b_{3N-3}(t)$$
$$+a'_4(t)b_4(t) + a'_7(t)b_7(t) + \cdots + a'_{3N-2}(t)b_{3N-2}(t). \quad (22)$$

Eq. 1 implies that each term in the bottom line of Eq. 22 is nonnegative, and consequently the sum of the terms in the right-hand side of the top line of Eq. 22, denoted $p(t)$, is nonpositive. This statement is written formally as

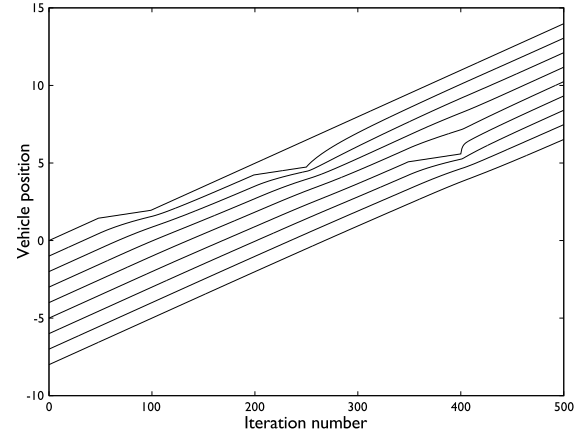$$p(t) = a'_2(t)b_2(t) + a'_3(t)b_3(t) + \cdots + a'_{3N-3}(t)b_{3N-3}(t) \leq 0. \quad (23)$$

Fig. 1. Discrete-time simulation results for $N = 9$, with $f_k(d_k(t)) = \ln(d_k(t))$, $k = 2,\ldots,9$, $g_k(d_{k+1}(t)) = \ln(d_{k+1}(t))$, $k = 1,\ldots,8$, and with the systems h_k being realized as discrete-time approximations to continuous-time integrators, corresponding to vehicles having speed control systems that compensate the vehicle dynamics so that $v_k(t) \propto b_{3k-2}(t)$. The associated cost terms in (18) are $F_k(d_k) = G_k(d_k) = (\ln d_k - 1)d_k$, i.e. with a minimum point at $d_k = 1$ and with distances less than 1 incurring greater cost than distances that are greater than 1. The systems h_k, $k = 1,\ldots,9$ are all identical, with the exception of h_6, which has a larger constant of integration than the others, representing perhaps a higher-performance vehicle that has the ability brake and accelerate more suddenly. Vehicle 1 is manually perturbed at iteration step 50, vehicle 2 is manually perturbed at iteration step 100, and vehicle 6 is manually perturbed at iteration step 350, with the duration of each perturbation being 50 iteration steps.

We observe that $p(t)$ is the time derivative of the cost function in (18), resulting in

$$\frac{d}{dt}\left(G_1(d_2(t)) + F_N(d_N(t)) + \sum_{k=2}^{N-1} F_k(d_k(t)) + G_k(d_{k+1}(t))\right)$$
$$= g_1(d_2(t))d'_2(t) + f_N(d_N(t))d'_N(t)$$
$$+ \sum_{k=2}^{N-1} f_k(d_k(t))d'_k(t) + g_k(d_{k+1}(t))d'_{k+1}(t)$$
$$= b_2(t)a'_2(t) + b_{3N-3}(t)a'_{3N-3}(t)$$
$$+ \sum_{k=2}^{N-1} b_{3k-3}(t)a'_{3k-3}(t) + b_{3k-1}(t)a'_{3k-3}(t)$$
$$= p(t) \leq 0.$$
$$(24)$$

The form of (18) illustrates the sense in which the presented architecture deals with measurement inconsistencies gracefully. Specifically, any inconsistencies in resource difference measurements can be factored into the functions $g_k(x)$ and $f_k(x)$, causing the overall system to reach an equilibrium point that differs from that of a system having consistent measurements, although does not result in instabilities.

4. SIMULATION RESULTS

A discrete-time simulation of the architecture is depicted in Fig. 1, illustrating that the effects of position perturbations die out as the chain recovers. Future work includes performance evaluation of the architecture in other situations that may be encountered in practice.
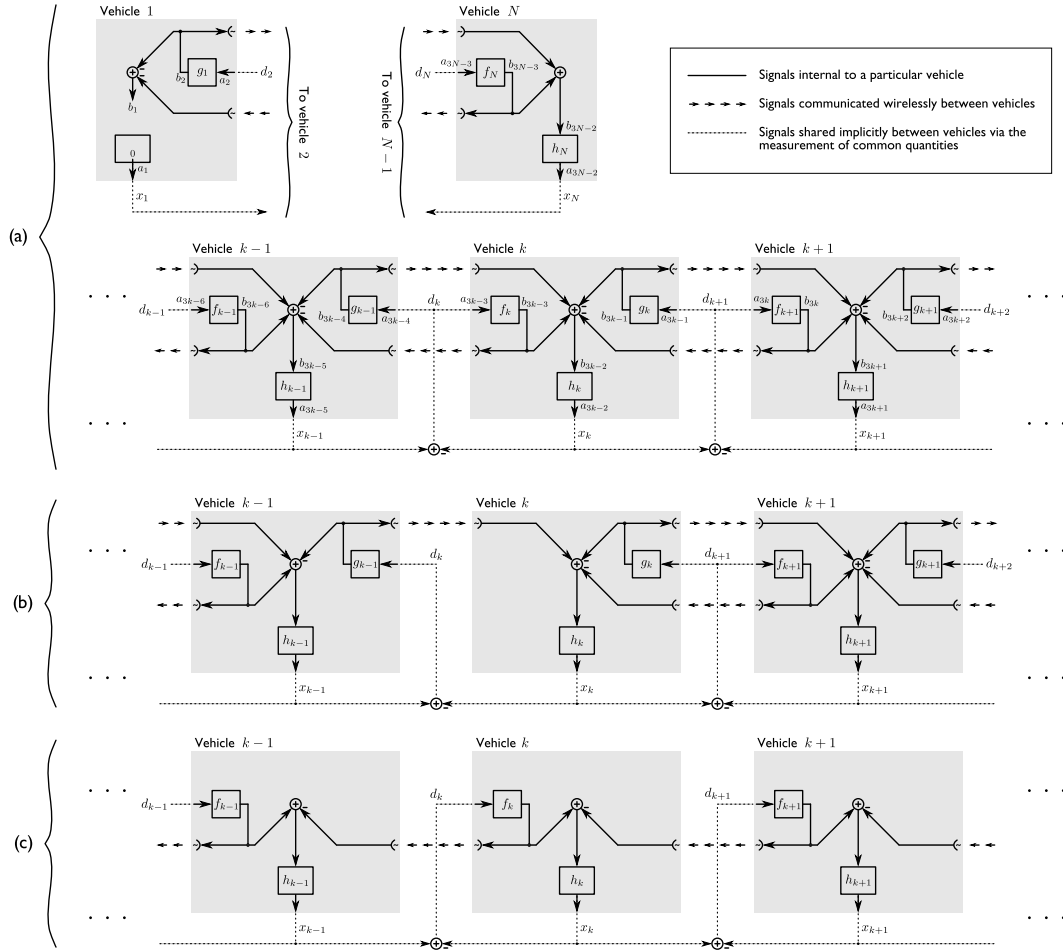
Fig. 2. (a) General architecture. (b) Implementation where the front-facing distance measurement in vehicle k is not used. (c) Implementation consisting of vehicles using exclusively front-facing distance measurements.
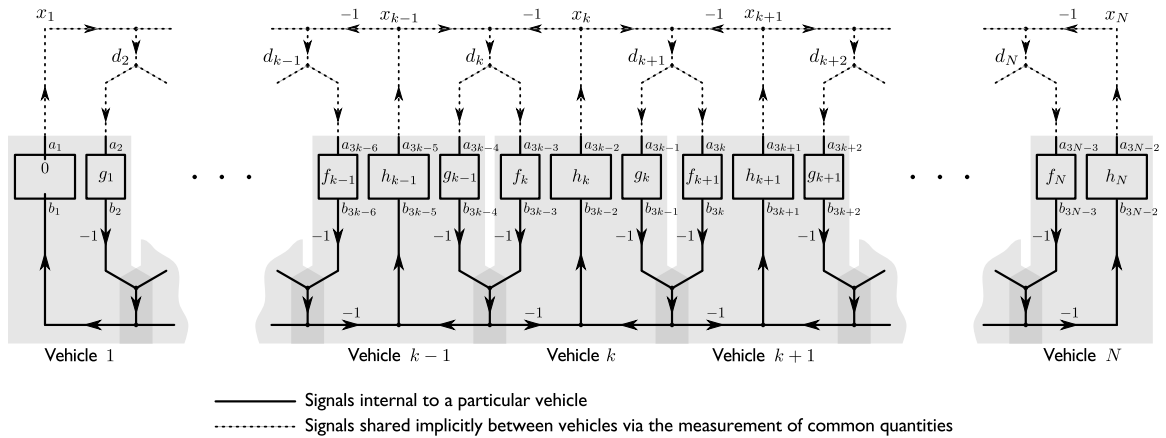

Fig. 3. Representation of the architecture in Fig. 2(a) in a form that facilitates the identification of a conservation principle. Light gray regions indicate portions of the system that are implemented within vehicles. Dark gray regions indicate signals that are shared between adjacent vehicles via a wireless link.

5. REFERENCES

[1] B. D. Greenshields, "A study of traffic capacity," in *Proceedings of the Highway Research Board*, 1935, vol. 14, pp. 448–477.

[2] M. Lighthill and G. Whitham, "On kinematic waves. ii. a theory of traffic flow on long crowded roads," in *Proceedings of the Royal Society – series A*, May 1955, vol. 229, pp. 317–345.

[3] G. Newell, "Mathematical models for freely-flowing highway traffic," *Operations Research*, vol. 3, no. 2, pp. 176–186, May 1955.

[4] P. I. Richards, "Shock waves on the highway," *Operations Research*, vol. 4, pp. 42–51, 1956.

[5] L. Edie and R. Foote, "Traffic flow in tunnels," in *Proceedings of the Highway Research Board*, 1958, vol. 37, pp. 334—344.

[6] H. Greenburg, "An analysis of traffic flow," *Operations Research*, vol. 7, no. 1, Jan/Feb 1958.

[7] R. Chandler, R. Herman, and E. Montroll, "Traffic dynamics: Studies in car following," *Operations Research*, vol. 6, no. 2, pp. 165–184, 1958.

[8] R. Herman, E. Montroll, R. Potts, and R. Rothery, "Traffic dynamics: Analysis of stability in car following," *Operations research*, vol. 7, no. 1, pp. 86–106, 1959.

[9] L. Edie, "Car-following and steady-state theory for noncongested traffic," *Operations Research*, vol. 9, no. 1, pp. 66–75, 1951.

[10] I. Priogine and R. Herman, *Kinetic Theory of Vehicular Traffic*, Elsevier, New York, 1971.

[11] J. Treiterer and J. Myers, "Hysteresis phenomenon in traffic flow," in *Proceedings of the 6th International Symposium on Transportation and Traffic Theory*, D. Buckley, Ed., New York, 1974, pp. 13–38, Elsevier.

[12] K. Nagel and M. Schreckenberg, "A cellular automaton model for freeway traffic," *Journal of Physics I (France)*, vol. 2, pp. 2221, 1992.

[13] G. Newell, "A simplified theory of kinematic waves in highway traffic, i. general theory, ii. queuing at freeway bottlenecks, iii. multidimensional flows," *Transportation Research*, vol. 27B, pp. 281–313, 1993.

[14] B. Kerner and H. Rehborn, "Experimental properties of phase transitions in traffic flow," *Physical Review Letters*, vol. 79, pp. 4030, 1997.

[15] C. Dagazano, M. Cassidy, and R. Bertini, "Possible explanations of phase transitions in highway traffic," *Transportation Research Part A*, vol. 33, pp. 365, 1999.

[16] D. Helbing and M. Schreckenberg, "Cellular automata simulating experimental properties of traffic flow," *Physical Review E*, vol. 59, pp. R2505, March 1999.

[17] K. Nagel, "Hell on wheels," *The Sciences*, p. 26, 1999.

[18] P. Weiss, "Stop-and-go science," *Science News*, vol. 156, no. 1, pp. 8–10, July 1999.

[19] P. Ball, "Slow, slow, quick, quick, slow," *Nature Science Update*, vol. 20, pp. 1858–1864, April 2000.

[20] T. Nagatani, "Traffic jams induced by fluctuation of leading car," *Physical Review E*, vol. 61, pp. 3534–3540, April 2000.

[21] I. Peterson, "Traffic woes of the single driver," *Science News*, vol. 157, pp. 153, May 2000.

[22] E. Tomer, L. Safonov, and S. Havlin, "Presence of many stable nonhomogeneous states in an inertial car-following model," *Physical Review Letters*, vol. 84, pp. 382–385, Jan 2000.

[23] I. Peterson, "Math trek: Waves of congestion," *Science News*, vol. 221, Sep 2001.

[24] D. Gazis, "The origins of traffic theory," *Operations Research*, vol. 50, no. 1, pp. 69–77, Jan/Feb 2002.

[25] S. Begley, "A few computer-controlled cars can help traffic," *Wall Street Journal*, July 2004.

[26] L. Davis, "Effect of adaptive cruise control systems on traffic flow," *Physical Review E*, vol. 69, June 2004.

[27] J. Minkel, "The computer minds the commuter," *Physical Review Focus*, June 2004.

[28] I. Peterson, "Math trek: Cruise control and traffic flow," *Science News*, Nov 2004.

[29] B. S. Kerner, *Introduction to Modern Traffic Flow Theory and Control*, Springer, New York, 2000.

[30] J. A. Laval and L. Leclerq, "A mechanism to describe the formation and propagation of stop-and-go waves in congested freeway traffic," *Philosophical Transactions Royal Society A*, vol. 368, no. 1928, pp. 4519–4541, 2010.

[31] B. K. P. Horn, "Saving energy by suppressing traffic flow instabilities," http://people.csail.mit.edu/bkph/talkfiles/Traffic_Instabilities.pdf, May 2012.

[32] V. Gupta, C. Langbort, and R.M. Murray, "On the robustness of distributed algorithms," in *Decision and Control, 2006 45th IEEE Conference on*. IEEE, 2006, pp. 3473–3478.

[33] R.M. Murray, "Recent research in cooperative control of multivehicle systems," *Journal of Dynamic Systems, Measurement and Control*, vol. 129, no. 5, pp. 571–583, 2007.

[34] T. A. Baran, *Conservation in Signal Processing Systems*, Ph.D. thesis, Massachusetts Institute of Technology, 2012.

[35] P. Penfield, R. Spence, and S. Duinker, *Tellegen's Theorem and Electrical Networks*, The MIT Press, Cambridge, Massachusetts, 1970.

[36] W. Millar, "Some general theorems for non-linear systems possessing resistance," *Philosophical Magazine*, vol. 42, no. 333, pp. 1150–1160, 1951.

[37] J. L. Wyatt, "Little-known properties of resistive grids that are useful in analog vision chip designs," *Vision Chips: Implementing Vision Algorithms with Analog VLSI Circuits*, pp. 72–89, 1995.

[38] J. L. Wyatt, C. Keast, D. Seidel, D. Standley, B. K. P. Horn, T. Knight, C. Sodini, H. S. Lee, and T. Poggio, "Analog VLSI systems for image acquisition and fast early vision processing," *International Journal of Computer Vision*, vol. 8, no. 3, pp. 217–230, Nov 1992.

[39] A.V. Oppenheim and R.W. Schafer, *Discrete-Time Signal Processing*, Prentice-Hall, Inc., Englewood Cliffs, NJ, third edition, 2010.